Poly(lactic acid) bio-composites containing biochar particles: Effects of fillers and plasticizer on crystallization and thermal properties

T. Haeldermans[1,3,4*], *P. Samyn*[1], *R. Cardinaels*[2], *D. Vandamme*[1], *K. Vanreppelen*[4], *A. Cuypers*[5], *S. Schreurs*[3]

[1]Research Group of Analytical and Applied Chemistry, IMO, Hasselt University, Diepenbeek, Belgium
[2]Polymer Technology, Eindhoven University of Technology, Eindhoven, The Netherlands
[3]Research Group Nuclear Technology, CMK, Hasselt University, Diepenbeek, Belgium
[4]Act&Sorb, BVBA, Genk, Belgium
[5]Research Group of Environmental Biology, CMK, Hasselt University, Diepenbeek, Belgium

Abstract. Biochar has emerged as a filler material for bio-degradable composites with favorable thermal and mechanical properties. Therefore, biochar is used in poly (lactic acid) (PLA) and PLA/thermoplastic starch (TPS) based composites. The crystallization and thermo-analytical properties of these blends with increasing amounts (20 to 50 wt%) of biochar are investigated. In the thermogravimetric analysis, the PLA/char composites' onset degradation temperature and temperature of maximum weight loss decrease with increasing biochar concentrations (320 to 275 °C and 380 to 350 °C, respectively). Contrastingly, in the PLA/TPS/char composites, the impact of the biochar is shielded by the TPS. The unaltered glass transition demonstrates that biochar does not act as a plasticizer in any of the composites, while TPS does. Biochar acts as a nucleation agent, but hinders further crystal growth at high concentrations, as confirmed by isothermal crystallization and infrared spectroscopy. The TPS smoothens the PLA/biochar interface, leading to an obstructed nucleation effect of biochar, proven by differential scanning calorimetry, infrared spectroscopy, and scanning electron microscopy. This work demonstrates the shielding effect TPS has on biochar and can help to understand further and optimize the production and biodegradability of these composites.

Keywords: polymer composites, thermal properties, biochar, polylactic acid, thermoplastic starch

1. Introduction

The use of biopolymers as sustainable replacements for fossil-based products is highly advantageous, as they are based on renewable resources and may have the additional benefit of biodegradability. One of the most researched biopolymers, poly (lactic acid) (PLA), has received much attention and became industrially viable because of its excellent mechanical properties and economically favorable renewable synthesis route, *e.g.*, via fermentation of starch. There are, however, some shortcomings to pure PLA like brittleness,

poor heat resistance, poor toughness, high costs, and poor biodegradability due to its high T_g, which hinders its applicability in many areas [1–4]. Therefore, starch is often used as a bio-based and biodegradable plasticizer either to improve the toughness or to tune the interphase compatibility of PLA composites [4]. Certain PLA-based materials with natural, lignocellulosic fillers (usually fibers), as reinforcements in the resulting bio-composites, have shown to be able to resolve a lot of the mechanical issues while remaining a completely bio-degradable product [5–7].

The use of biopolymers as matrices for natural fibers to produce bio-composites is, therefore, growing in popularity and gaining increasing approval for many years [8]. Natural fibers like bamboo, coir, flax, hemp, and many more have already been studied extensively for their use in bio-composites [8–11]. Furthermore, natural particulate fillers of various shapes (*e.g.* grape stem and alfalfa) were previously produced from different agricultural waste products and used in PLA composites with concentrations up to 50 wt% [12]. Although good results are often achieved, there are several reported problems with these fillers, including their hydrophilic nature, variation in quality, low mechanical properties, and sometimes high price [13]. Except for their price, the most serious reported shortcoming of natural fibers is their hydrophilic nature, causing fragile interfacial bonding between the fibers and the often hydrophobic polymers [14]. Furthermore, the various impurities, quality variations, and abundance of hydroxyl groups present on the fiber surface restrain the usability of natural fibers as reinforcement materials [15]. To resolve this, several post-treatments for these fibers have been suggested to modify their surfaces like alkali treatment, peroxide treatment, fungal treatment, and steam explosion [16]. Additionally, coupling agents can be used to improve adhesion between the fibers and certain polymers, increasing mechanical properties significantly [17].

Biochar, which is obtained as a side-stream valorization product from organic residues, can be used as an alternative natural filler. The production of biochar is a process of dealkylation, dihydroxylation (or dehydrogenation), and aromatization of the initial residue streams [18]. After pyrolysis, a limited number of surface functional groups are present on the biochar, and the low hydrogen and oxygen contents of the biochar lead to relatively high hydrophobicity, as compared to its original precursor [19]. Evidently, the reported issues on particle distribution and dispersion within a hydrophobic polymer matrix could be resolved by using biochar as a natural filler. The biochar's surface properties can eventually be tuned by appropriate parameter selection of the pyrolysis process. Taking this into account, pyrolysis temperature for rice husk biochar was optimized, and increasingly better mechanical properties of high-density polyethylene/biochar composites were found with increasing pyrolysis temperatures up to 600 °C [20]. Because of all the described advantages,

biochar has been successfully incorporated within different types of polymers for improving their electrical, mechanical, thermal, and flame retardant properties [21–23]. Examples are biochar particles in poly(trimethylene terephthalate) (PTT), and poly(lactic acid) (PLA) combined with a terpolymer matrix, resulting in increased impact strength, viscosity, and heat deflection temperature as compared to the neat matrix [24]. In poly(vinyl alcohol) (PVA), biochar addition of up to 10 wt% resulted in a similar electrical conductivity as that of PVA composites with carbon nanotubes or graphene. Furthermore, biochar addition improved thermal stability, tensile modulus, and storage modulus [25]. In PLA, biochar addition has led to improved mechanical properties (elastic modulus and impact energy) [26]. Other polymers used for producing biochar composites with advantageous characteristics are, amongst others: PTT [27], polyesters [28], and polyamides [29].

An additional advantage of using biochar as a filler material in biodegradable polymers is envisaged in the fact that the resulting bio-composite can be used as a slow-release fertilizer either at the end of its life or as its intended purpose. Biochar-based biodegradable polymer composites have been previously used as a slow-release fertilizer, showing both positive and negative results [30, 31]. Since PLA is only poorly biodegradable, a slow-release fertilizer based on this polymer seems unlikely. However, to resolve this issue, thermoplastic starch (TPS) has emerged as a promising low cost, biobased blending material for PLA, reducing costs and increasing its biodegradation and hence, release rate [32–34]. To the author's knowledge, no studies have been performed on the use of biochar in PLA/TPS bio-composites. Therefore, a better understanding of the interaction between biochar particles and the PLA or PLA/TPS blend is needed as a primary background to facilitate the design of biopolymers as carriers for release compounds and the understanding of release mechanisms of the filler. In a future application step, the variations in the crystallinity of the host polymer in the presence of biochar as a filler may particularly alter the diffusion mechanisms, thermal stability, and degradation, as well as mechanical properties resulting in premature fracture or brittleness, and biodegradability.

In this work, the effect of biochar particles produced from pyrolysis of tree bark (*Pinus Sylvestris*) on the internal structure of PLA/char composites is

investigated; in particular, the crystallization and thermo-analytical properties with an increasing amount of biochar fillers as an active ingredient are detailed. Furthermore, the additional use of TPS as a processing agent has been investigated in PLA/TPS/char composites in order to reveal the synergistic effects on processing and the aforementioned characteristics of the composites. As a result, a maximum or optimum amount of biochar can be proposed depending on the control over crystallization mechanisms and processing.

2. Materials and methods
2.1. Materials
Poly(lactic acid) pellets consist of a multi-purpose extrusion-grade polymer (123-3D, Almere, The Netherlands) with molecular weight $M_n \approx 100\,000$ g/mol, $M_w \approx 150\,000$ g/mol, melt index = 9.56 g/10 min (210 °C, 2.16 kg, ISO 1133), and copolymerization of L-lactic acid with < 4.5 to 5 wt% D-lactic acid. TPS (FlourPlast GP2) powder was bought from Rodenburg Biopolymers (Oosterhout, The Netherlands). The biochar was produced in our laboratories from tree bark (*Pinus sylvestris*), using a pilot-scale pyrolysis reactor at 450 °C and a residence time of around 12 min, as described in previous work [35]. Biochar was ground and sieved using a Retsch AS200 Basic sieving apparatus (Haan, Germany) to a particle size < 63 µm (mean size = 18.86 µm, lower 10% of the particles is below 4.80 µm, upper 10% of the particles is above 59.98 µm). The biochar was physicochemically characterized by ultimate analysis using a Thermo Electron Flash EA1112 elemental analyzer (Thermo Electron, Waltham, USA). Calibration was carried out using BBOT (2,5-bis(5-tert.-butyl-benzoxazol-2-yl)thiophene). Ash content was analyzed using ASTM E 1755 – 01. Oxygen was calculated by difference (O = 100% – C% – H% – N% – Ash%). As can be seen in Table 1, the biochar consists mostly out of carbon (70%), followed by oxygen (18%) and minerals (8%). The nitrogen and hydrogen content is limited to <1% and <3% respectively.
The most commonly found surface functionalities in FTIR are derived from aromatic C–H, and to a lesser extent, from inorganic carbonates and residual C–O

Table 2. Pre-mixed composition of PLA/char and PLA/TPS/char composites. TPS = Thermoplastic starch.

Sample	PLA [wt%]	TPS [wt%]	Biochar [wt%]
PLA	100	0	0
PLA/TPS 25/75	25	75	0
PLA/TPS 50/50	50	50	0
PLA/char 80/20	80	0	20
PLA/char 70/30	70	0	30
PLA/char 60/40	60	0	40
PLA/char 50/50	50	0	50
PLA/TPS/char 40/40/20	40	40	20
PLA/TPS/char 35/35/30	35	35	30
PLA/TPS/char 30/30/40	30	30	40
PLA/TPS/char 25/25/50	25	25	50

and C–OH groups from the biomass. The BET specific surface area of the used biochar is 2.40 m²/g (Table 1), as determined by using the N_2 adsorption and desorption isotherms at 77 K with a Tristar II 3020 surface area analyzer (Micromeritics, Georgia, U.S.A). All materials were dried overnight in a circulating hot air oven at 80 °C and sealed before further processing.
The different compositions of PLA/char and PLA/TPS/char were prepared according to Table 2, with both series having the same char content relative to either the PLA or the PLA/TPS polymer content. The compositions were pre-mixed in the required weight ratio's as a dry powder and subsequently compounded by melt-extrusion in a batch twin-screw microcompounder (DSM Xplore, Geleen, The Netherlands) at a temperature of 200 °C, a screw speed of 200 rpm, and a mixing time of around 5 minutes. The materials were collected as continuous strands, cooled under air conditions, and cut. All compositions were independently produced in threefold, broken down in small strands, and mixed into one batch.

2.2. Methods
Differential scanning calorimetry
Differential scanning calorimetry (DSC) was performed using a DSC Q200 (TA Instruments, New Castle, United Kingdom), running two heating cycles and an intermediate cooling cycle between –20 and 200 °C at a constant heating and cooling rate of

Table 1. Elemental composition of the used biochar.

Sample	N [%]	C [%]	H [%]	O [%]	Ash [%]	BET SSA [m²/g]
Biochar	0.86±0.02	70.27±0.89	2.77±0.04	18.03±0.89	8.08±0.08	2.40

20 °C/min using a sample mass of 10.0±0.1 mg. For isothermal crystallization, a sample mass of 10.0±0.1 mg was heated to the melting state at 200 °C and kept at this temperature for about 5 min to erase the thermal history, before the material was quenched at 100 °C/min to a crystallization temperature of 105 °C where it was kept for a period of 60 min. With the measured ΔH_m, the crystallinity level (X_c) can be determined according to Equation (1) [36]:

$$X_c = \frac{\Delta H_m}{(1 - \Phi)\Delta H_0} \cdot 100\% \tag{1}$$

where ΔH_0 is the ΔH_m of entirely crystallized PLA (106 J/g) [37], and Φ is the weight fraction of the filler.

Thermogravimetric analysis
Thermogravimetric analysis (TGA) (TA Instruments Q500, Zellik, Belgium) was performed on a sample mass of 10.0±0.1 mg during heating from room temperature to 550 °C at a heating rate of 20 °C/min under 90 ml/min N$_2$-flow.

Fourier transform infrared spectroscopy
FT-IR spectra were obtained using a VERTEX 70 FTIR spectrometer equipped with a DTGS detector (Bruker, Karlsruhe, Germany), in attenuated total reflection (ATR) mode using a diamond crystal. The spectra were collected between 4000–600 cm^{-1} at a resolution of 4 cm^{-1} and averaged over 32 scans per sample. The total crystallinity of the PLA/Char samples can be estimated by Equation (2) [38]:

$$X_{c(FTIR)} = \frac{I_{920\,cm^{-1}}}{I_{920\,cm^{-1}} + I_{955\,cm^{-1}}} \cdot 100\% \tag{2}$$

where $I_{920\,cm^{-1}}$ and $I_{955\,cm^{-1}}$ are the areas of the crystalline and amorphous bands, respectively.

Scanning electron microscopy
The morphology of the composites was evaluated by using a TM3000 Tabletop Scanning Electron Microscope at 15 kV (Hitachi, Krefeld, Germany). Samples were cryo-fractured from the produced strands into smaller parts and were gold sputter-coated using a jfc-1300 auto fine coater (Jeol, Tokyo, Japan) for 60 seconds at 30 mA, 0.05 mbar, and a working distance of 4 cm.

3. Results and discussion
3.1. Thermogravimetric analysis
In Figure 1, the thermal stability of PLA/char and PLA/TPS/char composites is shown. It can be seen that pure PLA decomposes in the temperature range from 320 to 395 °C. The maximum weight loss occurs at 380 °C, which is the highest among all compositions. The onset degradation temperature of the PLA/char composites is lower than this of pure PLA and systematically decreases with the amount of filler material. With 20% of biochar filler, the start of the degradation and the maximum degradation temperature lower to about 290 and 365 °C, respectively, while this is about 275 and 350 °C for 50% of biochar filler. This decrease in onset and maximum degradation temperature was previously found for both organic and inorganic fillers in PLA [39–44]. It is likely caused by the decrease in molecular weight during processing of the composites, which is accelerated in presence of fillers. After all, when biochar is added to the samples, the melt shear viscosity increases, thereby elevating the shear stress on the polymer chains as well as the internal heating due to friction and therefore accelerating degradation during processing [39]. Additionally, carbonates originating from the biochar may have a catalytic effect on the degradation of the ester bonds of PLA [42]. After PLA has completely degraded ($T > 400$ °C, Figure 1b), the residual mass is considered as biochar filler in the PLA/char samples. As such, the amounts of biochar filler as determined by TGA at 450 °C in the PLA/char samples are 19.7% (PLA/char 80/20), 27.2% (PLA/char 70/30), 38.5% (PLA/char 60/40), and 44.3% (PLA/char 50/50) respectively (Table 3). Any additional mass loss after 450 °C is originating from the degradation of the biochar.
The same results can be obtained from the PLA/TPS/char samples after both PLA and TPS have degraded completely (500 °C, Figure 1d). The amounts of biochar in the PLA/TPS/char samples as determined by TGA and taking the remaining amount of TPS (13.64% in the pure TPS sample) at 500 °C into account are respectively 19.4% (PLA/TPS/char 40/40/20), 26.0% (PLA/TPS/char 35/35/30), 34. % (PLA/TPS/char 30/30/40) and 43.7% (PLA/TPS/char 25/25/50) (Table 3). Duplo measurements in both PLA/char and PLA/TPS/char yield errors below 0.1%. It can therefore be concluded that the amount
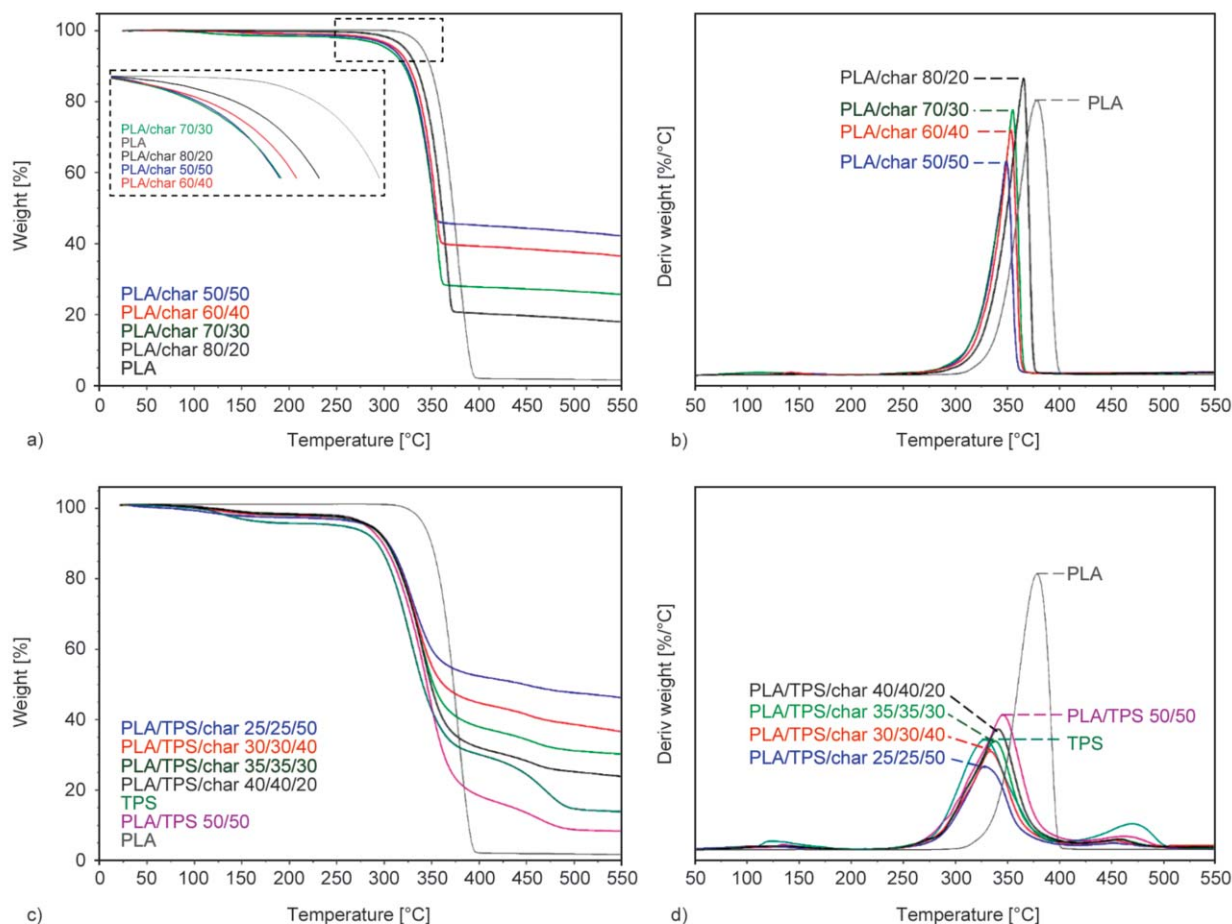
Figure 1. Thermogravimetric and differential thermogravimetric analysis of the PLA/char composites (a, b, respectively) and the PLA/TPS/char composites (c, d, respectively) in the temperature range of 20 to 550 °C under nitrogen atmosphere.

of biochar is comparable with the original formulation of the composites, which confirms good homogeneity of the samples with distributive mixing of the biochar fillers, while the retention of char in the matrix has improved in the presence of TPS. Deviations between the applied and resulting mixture ratios occurred due to processing and equipment limitations (e.g. volatilization of very fine biochar particles and residual material in the hopper).

All PLA/TPS/char compositions with a similar ratio of PLA/TPS 50/50 show an initial weight loss between 50 and 200 °C, corresponding to water loss and volatilization of the plasticizer in TPS [45]. The onset degradation temperature for PLA/TPS has dropped to lower values than that of the pure PLA because of the decomposition of the present starch [45]. Contrary to the PLA/char composites, the influence of the biochar on the onset degradation temperature of the PLA/TPS/char composites is negligible, as all the composites with biochar start their decomposition at the same temperature (around 265 °C) as PLA/TPS

50/50. Although the onset degradation temperature is the same for all samples, the temperature of max weight loss is decreasing from 340 °C in PLA/TPS/char 40/40/20 to 328 °C in PLA/TPS/char 25/25/50, which is less pronounced as compared to PLA/char composites (Figure 1d). Based on these observations, it can be concluded that, when TPS is present in PLA/ TPS/char, the influence of the biochar particles on the onset degradation temperature of the composites is no longer visible, while the presence of TPS dominates.

3.2. Differential scanning calorimetry
Nonisothermal characterization
To further understand the influence of biochar on the thermal behavior of the PLA/char and PLA/TPS/ char composites, DSC analysis is performed. First, the influence of biochar on the glass transition behavior is discussed, then the influence on the melting behavior and degree of crystallinity is determined from the heating cycles in regular DSC scans. Finally,

as nonisothermal crystallization is not occurring at the applied cooling rate in DSC (20 °C/min), isothermal crystallization is performed to assess the influence of the biochar particles as an active filler on the crystallization kinetics and mechanisms of the composites.
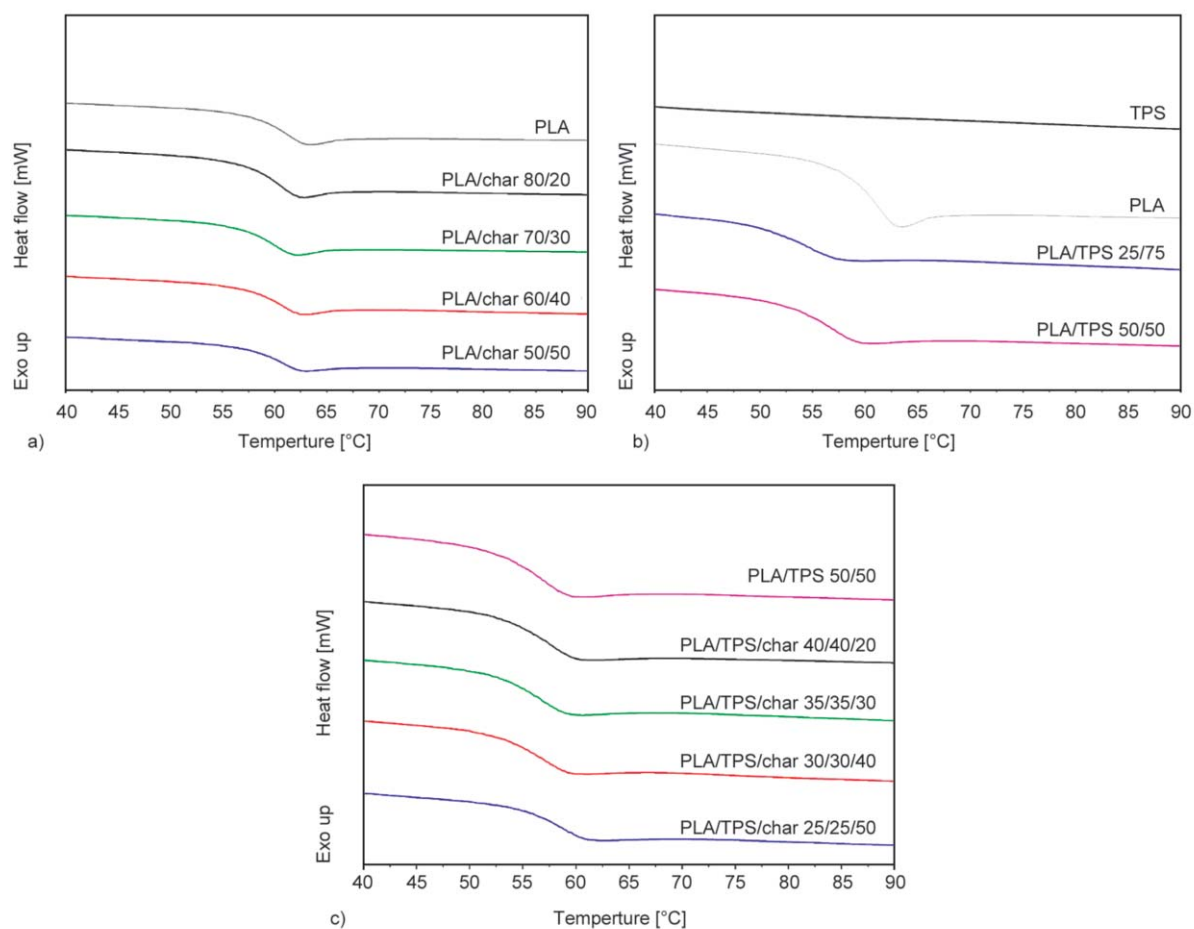
Figure 2. Thermal behavior of PLA/char composites in the T_g region (a), thermal behavior of PLA/TPS composites in the T_g region (b) and thermal behavior of PLA/TPS/char composites in the T_g region (c). All graphs represent the second heating cycle in DSC.

Table 3. Thermal characteristics of all composite materials. T_g is glass transition temperature (measured in the second heating cycle in DSC), ΔC_p is glass transition enthalpy (measured in the second heating cycle in DSC and normalized for the PLA content), T_m is melting temperature (measured in the first heating cycle in DSC) and ΔH_m is melting enthalpy (measured in the first heating cycle in DSC and normalized for the PLA content), X_c is the crystallinity level, TPS is Flourplast. (–) indicates that no result is available.

Sample	Biochar [%]	T_g [°C]	ΔC_p [J/g]	T_m [°C]	ΔH_m [J/g]	X_c [%]	X_{cFTIR} [%]
PLA	0	63.2	2.1	150.0	36.2	31.3	57.4
TPS	0	–		–	–	–	–
PLA/TPS 50/50	0	59.5	1.4	145.7	32.6	30.8	–
PLA/TPS 25/75	0	57.2	2.8	145.3	56.4	53.0	–
PLA/char 80/20	19.7	62.4	2.2	152.9	45.4	42.8	36.2
PLA/char 70/30	27.2	61.9	2.4	149.8	37.6	35.5	44.0
PLA/char 60/40	38.5	62.4	2.3	148.2	38.2	36.0	2.7
PLA/char 50/50	44.3	62.6	2.4	148.4	36.7	34.6	12.1
PLA/TPS/char 40/40/20	24.9	59.9	1.4	147.4	36.5	34.3	–
PLA/TPS/char 35/35/30	30.8	59.1	1.7	145.4	38.9	36.7	–
PLA/TPS/char 30/30/40	38.2	59.2	1.9	145.4	45.0	42.2	–
PLA/TPS/char 25/25/50	47.1	61.2	1.7	149.0	37.6	35.34	–

A detail from the nonisothermal DSC analysis illustrates the effect of biochar fillers on the glass transition temperature (T_g) and heat capacity change (ΔC_p) for PLA/char and PLA/TPS/char composites, shown in the thermographs in Figure 2 and summarized as numerical values in Table 3. When biochar particles are added to the PLA matrix, no significant influence on the glass transition temperature (T_g) of PLA is observed (Figure 2a). The T_g remains within a statistical temperature variation of 1 °C, and therefore no plasticizing effect of biochar on PLA is observed. In parallel to the changes in T_g, the normalized glass transition enthalpy (ΔC_p) remains generally unaffected by the biochar particles as it remains between 2.2 and 2.4 J/g in all PLA/char samples, as compared to 2.1 J/g for pure PLA.

In the presence of TPS, the T_g of PLA is significantly decreased from 63.2 for pure PLA to 59.5 °C for PLA/TPS 50/50 and to 57.2 °C for PLA/TPS 25/75, respectively (Figure 2b). This indicates that TPS is well dispersed in the composite and therefore allows for a lower T_g. The plasticizing effect of TPS is well-known

[32], and the resulting reduction in T_g is far more pronounced than for biochar fillers. Adding biochar to the PLA/TPS samples again has no significant effect on the T_g of the PLA/TPS/Char composites as the deficit in T_g remains below or around 1 °C. At high biochar concentrations, the biochar particles are even counteracting the plasticizing effect of the TPS on PLA, most likely due to the fact that a large amount of biochar particles restrict the mobility of the polymer. The normalized glass transition enthalpy (ΔC_p) first increases to 1.9 J/g in PLA/TPS/char 30/30/40 and then decreases again to 1.7 J/g in PLA/TPS/char 25/25/50, confirming that the chain gradually becomes more mobile due to the presence of TPS, while being restricted at the highest char concentrations (50 wt%).

The effects of biochar on the melting temperature (T_m) and degree of crystallinity (X_c) can be followed from the melting trajectories shown in the thermograms in Figure 3 and summarized integration values included in Table 3. From Figure 3a, it can be seen that the melting temperature of PLA in the first heating
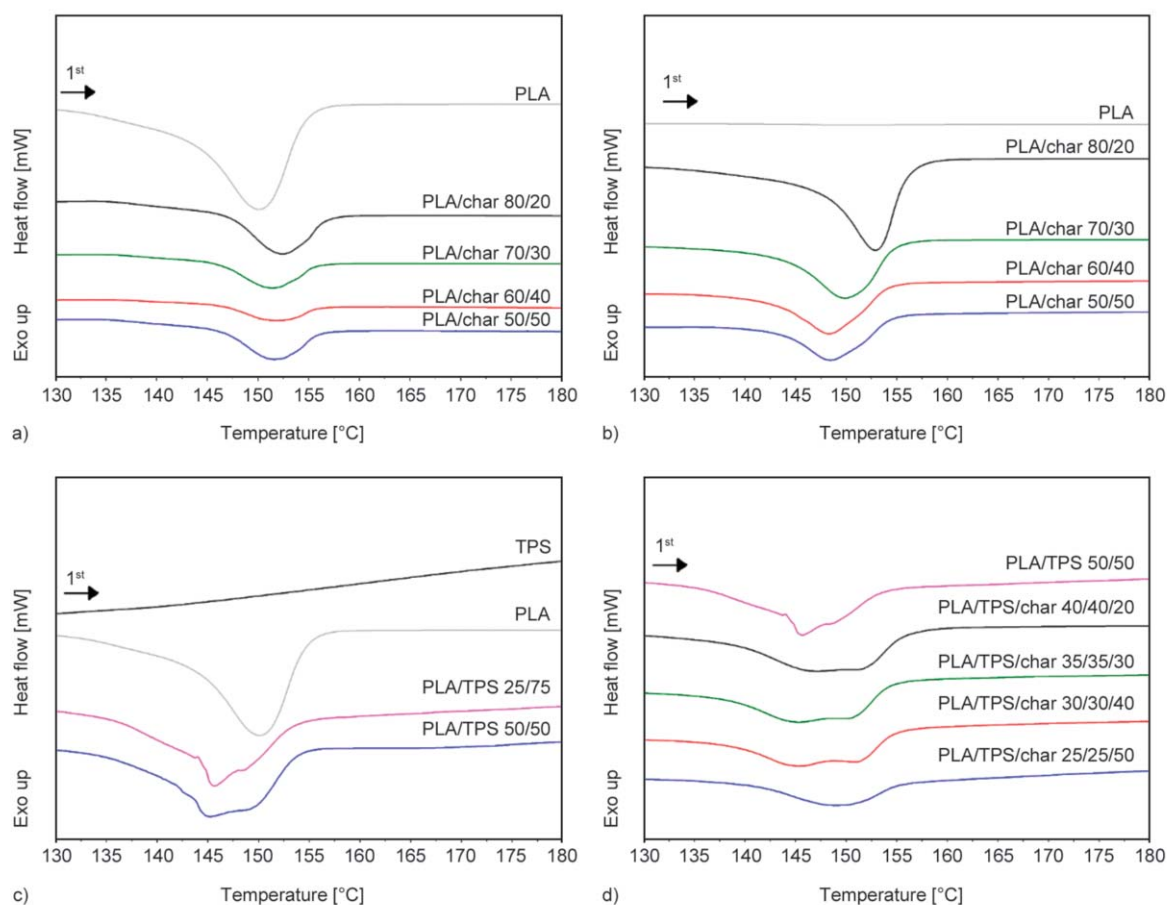
Figure 3. Thermal behavior of all composites in the melting temperature range with: the first heating DSC curves of PLA/char samples (a), the second heating DSC curves of PLA/char samples (b), the first heating DSC curves of PLA/TPS samples (c) and the first heating DSC curves of PLA/TPS/char samples (d).

cycle first increases from 150.0 °C for pure PLA to 152.9 °C in PLA/char 80/20, and then decreases with an increasing amount of biochar to 148.4 °C in PLA/char 50/50, due to interaction between PLA and biochar particles. In parallel, the normalized melting enthalpy (ΔH_m) of the composite materials first decreases sharply from 45.4 J/g in PLA/char 80/20 to 37.6 J/g for PLA/char 70/30 and then remains relatively constant with an increasing amount of added filler, but always remains higher than this of pure PLA (Table 3). It has to be noted that the first heating cycle is recorded after extrusion, which provides a characterization of the material after processing. Consequently, chain orientation caused by flow during extrusion may not be completely relaxed before solidification of the material. To ensure a consistent thermal and flow history for all materials, samples for DSC were always taken at the same distance from the beginning of the strand.

For PLA without any fillers, no melting peak was observed in the second heating cycle (Figure 3b). This corroborates with the lack of a crystallization peak during the cooling scan of PLA (details not shown), which is a common feature for commercial grades of pure PLA due to the relatively slow nucleation and crystallization growth mechanism by the organization of the PLA chains. A melting peak did, however, always occur when biochar was added to the PLA matrix, proving the favorable crystallization effect biochar particles have on PLA. The melting peak in the second heating run remains relatively sharp and is located at higher temperatures at low biochar concentrations in PLA/char 80/20, while it progressively broadens and shifts towards lower temperatures with increasing biochar concentrations. This suggests that a small amount of biochar acts as a nucleating agent, while the crystalline quality or size reduces in the presence of higher biochar concentrations. For PLA composites with talc as a filler, it was hypothesized that the large nucleation rate of the filler leads to the formation of many small crystals that melt at a lower temperature [46]. This hypothesis is in accordance with the results for PLA with high amounts of biochar. The occurrence of the highest melting temperatures would be attributed to the formation of a denser crystalline structure by recrystallization processes, which is obviously hindered in the presence of biochar fillers. The highest melting temperatures were achieved for PLA/char 80/20 in both the first (152.9 °C) and the second heating cycle (152.3 °C).

Therefore, the melting behavior of the PLA related to the development of specific crystalline structures is clearly influenced by the presence of biochar fillers. From Table 3, it is clear that for the biochar composites, X_c is always higher than this of the pure PLA. This indicates that biochar particles have a nucleation ability when incorporated in the PLA structure, thereby increasing the degree of crystallinity. Lezak *et al.* [47] previously found that high amounts of organic particles with developed surfaces act as a nucleating agent in PLA-based composites. Furthermore, similar results were previously found when chestnut shell biomass was used as a filler material at 30 wt% in PLA [48]. The reduction in melting temperature when more than 20 wt% of biochar is present in the sample, together with the reduction in X_c, rather suggests a reduction in crystallite stability or size due to a large amount of biochar particles, hindering the growth of the crystals. This confirms the previous hypothesis that the crystalline quality or size reduces in the presence of high biochar concentrations, as the presence of small microparticles likely hinders the molecular freedom and mobility to reorganize in a well-ordered crystalline structure.

Considering the effects of TPS (Figure 3c), it can be seen that TPS shows no melting behavior in the temperature range of 130–170 °C, and the PLA/TPS composites both show a double melting peak that becomes more intense for the PLA/TPS 50/50 than for the PLA/TPS 25/75. It is, therefore, clear that TPS has a significant influence on the crystallization process of PLA. Comparing PLA/TPS 50/50 and PLA/char 50/50, the influence of TPS on the crystallization of PLA seems to be larger than this of biochar, as the melting peak is split and broadened to a further extent. The double melting peak was previously found for PLA/(thermoplastic) starch blends and attributed to the plasticizer and nucleation effect of the (thermoplastic) starch [49, 50]. The occurrence of the double melting peak in PLA is commonly attributed to the crystalline polymorphs with a recrystallization process inducing the transformation of an α′-crystalline mesophase into a more stable α-crystalline phase, which is more favorably promoted by TPS in contrast to the biochar fillers. The double melting peak behavior is also visible in the first heating cycle of all PLA/TPS/char composites (Figure 3d), except for the composite with the least amount of TPS and the highest amount of biochar (PLA/TPS/char 25/25/50). The absence of this co-operative

melting peak in PLA/TPS/char 25/25/50 is attributed to the high level of biochar particles, which makes it harder for the TPS to assert a significant influence on the crystallization process of PLA. In the second heating cycle, no melting peak was observed for any of the PLA/TPS/char samples, confirming that no crystallization was achieved during the nonisothermal cooling cycle. In the PLA/char samples, a melting peak was indeed observed in the second heating cycle, indicating that TPS obstructed the nucleation effect of the char.

The influence of TPS and biochar on the crystallization of PLA is also visible in X_c (Table 3), as this parameter is rising from 31% in PLA to 53% in PLA/TPS 25/75. This observation is in agreement with the known behavior of TPS as a nucleating agent in composite materials [32]. A lot of research has already been done on the influence of (thermoplastic) starch in PLA composites on the crystallization of these composites. These studies all confirm and conclude that TPS does indeed act as a nucleation agent, improving the crystallinity of the PLA [33, 34, 51]. When adding both TPS and biochar, X_c is lower than

this of PLA/char composites at low char concentrations (20 wt%), again indicating the obstruction of the nucleation effect of the biochar. Crystallinity rises to a maximum of 42% at intermediate char concentrations in PLA/TPS/char 30/30/40 and then decreases again to 35% in PLA/TPS/char 25/25/50.

Isothermal characterization

The effect of biochar as an active filler on the crystallization kinetics of PLA/char composites was further detailed from isothermal crystallization experiments at 105 °C, as shown in Figure 4. The occurrence of crystallization over time can be noticed as an exothermic peak in the heat flow signal (Figure 4a), which remains absent for the pure PLA and shifts in time and/or intensity when biochar fillers are present. In the presence of biochar fillers, two concurrent effects likely manifest: *i.e.* the higher char concentrations accelerate the time for maximum crystallization while the intensity of the crystallization process decreases. The results of isothermal crystallization can be further described by the Avrami model to determine the kinetic crystallization parameters, as frequently used to
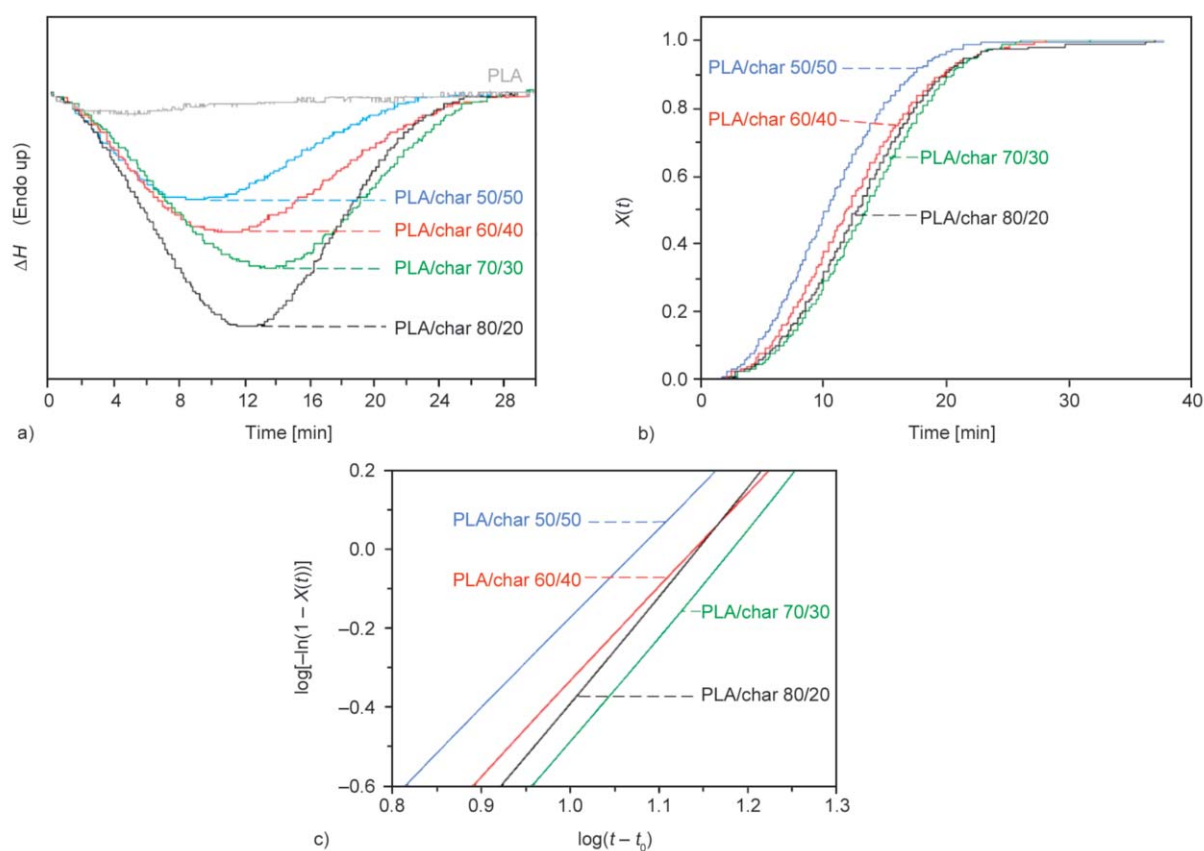
Figure 4. Isothermal crystallization isotherms of PLA/char composites (a), relative crystallinity *vs.* time (b) and the Avrami plots of log[–ln(1 – X_t)] *vs* log(t – t_0) for PLA/char composites cooled from melt to an isothermal crystallization temperature of 105 °C (c).

monitor the effects of nucleating agents (such as *e.g.*, phtalhydrazide) in PLA [52]. The Avrami equation is widely used to describe the isothermal crystallization of polymers and is given by Equation (3) [53]:

$$\log\left[-\ln(1-X_\mathrm{t})\right] = \log(k) + n \cdot \log(t) \quad (3)$$

where X_t is the time-dependent volume fraction of crystallinity (relative crystallinity), k is the crystallization constant [min^{-1}], and n is the Avrami exponent. The relative crystallinity Xt can be calculated from the experimental isothermal DSC heat flow measurements according to Equation (4):

$$X_\mathrm{t} = \frac{\int_0^t \frac{\mathrm{d}H}{\mathrm{d}t}\,\mathrm{d}t}{\int_0^\infty \frac{\mathrm{d}H}{\mathrm{d}t}\,\mathrm{d}t} \quad (4)$$

with $\mathrm{d}H/\mathrm{d}t$ the relative heat flow, as calculated by integration of the experimental isothermal crystallization experiment (Figure 4a). The latter plots of X_t *versus* $(t-t_0)$ (Figure 4b) exhibit a typical S-curve that illustrates the different stages of the crystallization process as a function of time. After logarithmic transformation, the plot of $\log[-\ln(1-X_\mathrm{t})]$ *vs* $\log(t-t_0)$ is linear in the selected range (Figure 4c), and the crystallization parameters k and n are determined by curve fitting the data (*i.e.*, slope n and intercept $\log(k)$). These crystallization parameters for PLA/char composites with different biochar percentages are summarized in Table 4.

Although the interpretation of the Avrami constants (k and n) is difficult and open to interpretation, important information can be gained from these parameters [53]. The Avrami exponent (n) is related to the dimensions of crystal growth and the nature of nucleation. The n values of the composite materials are between 2.73 and 2.27 and decrease with increasing

biochar content. An n value close to 3, as is the case for the samples with lower amounts of biochar, is an indication that the crystal growth is a three-dimensional and athermal process. Furthermore, this is an indication that the nuclei are preformed and present from the beginning. The lower values of *n* observed at higher biochar concentrations indicate the presence of non-randomly distributed nucleation sites, reducing the growth to 1 or 2 dimensions [54]. This is in good correlation with the high amounts of biochar particles (>30 wt%), hindering the growth of large crystals.

Analysis of the half crystallization time ($t_{1/2}$) indicates first that there is a good correlation between the experimentally found $t_{1/2}$ and the $t_{1/2}$ determined with the Avrami model. Secondly, there is a strong correlation between the $t_{1/2}$ with the amount of biochar in the composites. The faster crystallization rate that is achieved as more biochar is added to the sample is ascribed to the nucleation effect in the presence of biochar. It is noticeable that the $t_{1/2}$ keeps decreasing when more micro-scale biochar particles are added. Contrastingly, it was found that for nanoscale particles, this optimal crystallization rate is already achieved at 10 wt% of filler material, after which the $t_{1/2}$ increased again [55]. This optimum concentration is evidently higher for the micro-scale biochar particles, as it was also observed in the presence of talc or kenaf fiber [54, 56]. The higher optimum concentration required for the biochar particles is related to the specific interface area between the particle and matrix, where heterogeneous nucleation starts.

3.3. Fourier transform infrared spectroscopy

The FTIR spectra of PLA/char composites with different concentrations of biochar are shown in Figure 5a, indicating significant variations in the spectral range of 1900 to 600 cm^{-1}. The spectra were normalized on the 1455 cm^{-1} band (–CH$_3$) as it is centrally located and inert [42]. Furthermore, this absorption band is absent in the spectrum of the biochar. The characteristic bands for PLA are recognized and explained into detail in [38], while the biochar fillers only showed a specific absorption band in the region of around 1600 cm^{-1}. This broad band is increasing with the amount of biochar particles in both the PLA/char and PLA/TPS/char composites and is attributed to C=C aromatic ring stretching of the biochar, as was also found by Das *et al.* [22]. The FTIR fingerprint region can be used as a technique for

Table 4. Avrami kinetic crystallization parameters for the different PLA/char composites. In PLA, no crystallization was observed due to the lack of nucleating agents.

Sample name	n	k ($\cdot 10^{-4}$)	$t_{1/2}$ model [min]	$t_{1/2}$ exp [min]
PLA	–	–	–	–
PLA/char 80/20	2.73	8.34	12.63	12.50
PLA/char 70/30	2.70	7.28	12.72	13.26
PLA/char 60/40	2.39	18.89	11.84	10.83
PLA/char 50/50	2.27	35.76	10.16	8.90
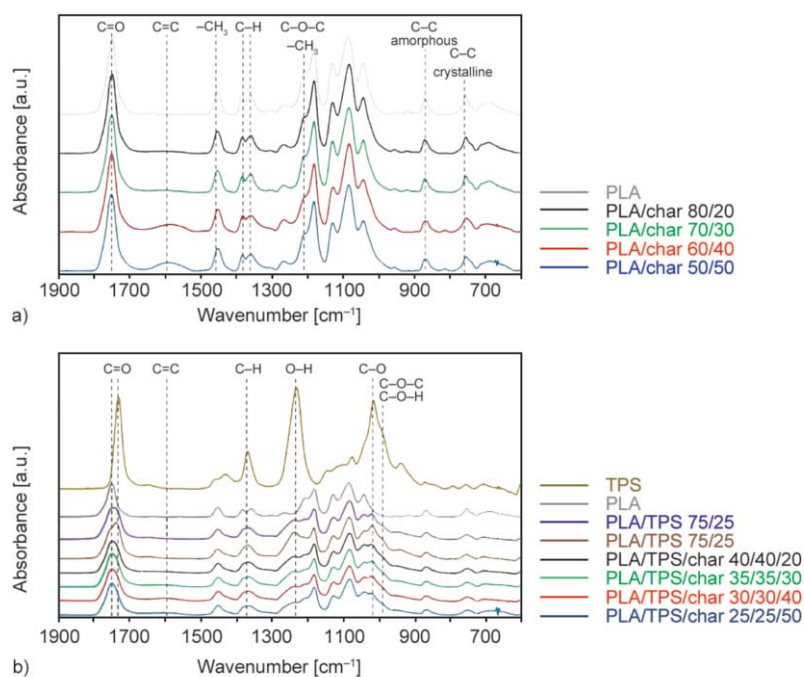
Figure 5. FTIR spectra in the region of 600–1900 cm^{-1} of PLA/char (a) and PLA/TPS/char (b) composites normalized at the intensity of the CH$_3$ band at 1455 cm^{-1}.

qualitative analysis of the crystalline structure (1000 to 1900 cm^{-1} spectral region) and estimation of quantitative crystallinity (especially in the 900 to 970 cm^{-1} spectral region).

From the spectral region 1000 to 1900 cm^{-1}, slight structural changes of the PLA polymer matrix upon the addition of biochar fillers are observed (Figure 5a). The 1777 cm^{-1} band (C=O ester) is the most intense and well-resolved peak, which does not show significant variations in intensity or position between the different composites. The minor influences of crystallinity in the 1777 cm^{-1} band with an eventual shift from 1743 cm^{-1} (amorphous) to 1783 cm^{-1} (crystalline) were not observed, as they mostly change after variation in interlamellar region spaces during thermal treatment after a relatively long time [57]. The 1382 and 1360 cm^{-1} bands (C–H stretching of –CH$_3$) do not specifically change with crystallinity [58], but changes in crystallinity might induce stress or orientation on the polymer side-chains. This is reflected by the decrease of the relative intensity of the 1360 cm^{-1} absorption band at higher biochar concentrations. The 1212 cm^{-1} shoulder band (C–O–C asymmetric vibrations, –CH$_3$ asymmetric rocking vibrations) is sensitive to conformational changes in the backbone and crystalline phase [57] and is significantly more pronounced in the spectrum of PLA, PLA/char 80/20, and PLA/char 70/30 than in the spectra of PLA/char 60/40 or PLA/char 50/50. These

variations indeed agree with the DSC measurements, indicating the highest degree of crystallinity for PLA/char 80/20 and PLA/char 70/30. In the lower wavenumber region, the 863 cm^{-1} bands (C–C, amorphous) and 758 cm^{-1} bands (C–C, crystalline) [59] indeed show slight changes that qualitatively can be related to small crystalline variations by the addition of char.

Supplementary effects with a TPS plasticizer are observed (Figure 5b), including an overlapping band originating from both the carbonyl stretching peak at around 1760 cm^{-1} of PLA and the corresponding TPS peak at around 1730 cm^{-1}, of which the ratio is changing in agreement with the composition. The aromatic C=C peak at around 1600 cm^{-1} originating from the biochar is masked by the presence of TPS. Furthermore, the influence of the biochar particles seems to be greater on TPS than on PLA. This is evidenced by the fact that the only changes that are occurring when more biochar is added to the composites are decreases in the characteristic bands of TPS at around 1365 cm^{-1} (C–H bending in CH$_2$ [60]), 1238 cm^{-1} (O–H bending [61]), 1020 cm^{-1} (C–O stretching of the anhydro-glucose ring of TPS [62]), 995 cm^{-1} (C–O–C stretching vibrations of α-1,4 glycosidic linkages and C–O–H bending vibrations [63]) (Figure 6). The bands at around 1212 and 1140 cm^{-1}, representing PLA crystallinity [57], do not decrease with biochar addition. This indicates that the influence
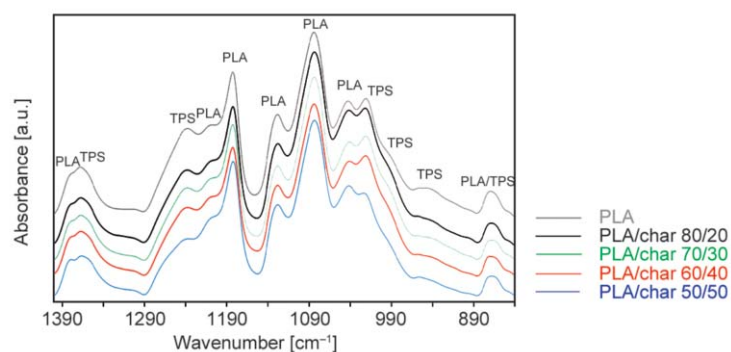
Figure 6. FTIR spectra in the region of 840–1400 cm^{-1} of PLA/TPS/char composites, normalized at the intensity of the CH_3 band at 1455 cm^{-1}. PLA indicates that the band is originating from PLA, TPS indicates that the band is originating from TPS.

of biochar on the crystallization of PLA is minimal as compared to that of TPS. Furthermore, the decreasing band at 1238 cm^{-1} with an increasing amount of biochar indicates that biochar interacts mostly with TPS via OH-interactions [61] in the polymer side chains, while the backbone stays unaffected by the biochar. This observation suggests that the interface between biochar and PLA is smoothened by the mediating effect of TPS.

A special region of interest for both PLA/char and PLA/TPS/char composites is the one between 900 and 970 cm^{-1} (Figure 7). The absorption band at 920 cm^{-1} is known as the characteristic of α crystals [64]. It was previously found that during crystalliza-
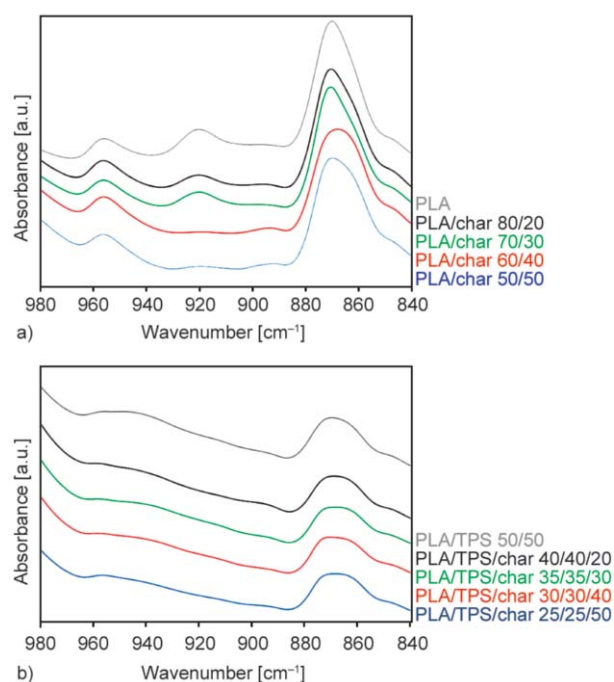
Figure 7. FTIR spectra in the 900–970 cm^{-1} region for PLA/char (a) and PLA/TPS/char (b) composite materials.

tion, the intensity of the band at 920 cm^{-1} increases, while the intensity of the amorphous band at 955 cm^{-1} decreases. These trends are indeed observed in the presence of biochar (Figure 7a), with more crystalline structures for PLA/char 80/20 and PLA/char 70/30 than in the PLA/char 60/40 or PLA/char 50/50. Although the decrease in crystallinity with the addition of more biochar in the PLA samples only occurs after more than 30 wt% of biochar in FTIR, the results correlate well with DSC as very high biochar contents decrease the overall crystallinity of the sample.

It is, therefore, possible to determine the quantitative relative crystallinity of the samples using the intensity ratios of both absorption bands [38].

The calculated values change from X_c = 57.4% for pure PLA, to X_c = 36. % (PLA/char 80/20) and X_c = 44.0% (PLA/char 70/30) and X_c < 10% for the PLA/char compositions with more biochar. In the PLA/TPS/char samples, no unambiguous quantitative information about $X_{c(FTIR)}$ can be obtained from these peaks due to the presence of the C–O–C vibration band of starch at around 930 cm^{-1} [65], causing strong overlap in the concerned region (Figure 7b). The stronger variations in crystallinity calculated from FTIR compared to DSC are due to the fact that both techniques detect different aspects of the crystalline structure [42]. However, the crystallization may be strongly influenced by interfacial interactions between the matrix and filler, forming very local crystallites or trans-crystalline layers with very complex melting behavior that differs from the properties of a spherulite-like crystalline phase. In particular, for the porous fillers, the nucleating ability and formation of the supramolecular structure are strongly influenced by the particle morphology [66].

3.4. Scanning electron microscopy

The changes in morphology for PLA, PLA/char, and PLA/TPS/char composites are illustrated by SEM microscopy on a fractured cross-section of the extruded strands. First, it is clear from Figure 8a that the used biochar is very heterogeneous, both in size and shape. The macroscopic surface of the used biochar is characterized by smooth regions, alternated with rough, porous regions due to degradation during pyrolysis. For the pure PLA (Figure 8b), a smooth and continuous polymer section is observed as biochar particles are not influencing the interface in this sample. For the PLA/char 80/20 (Figure 8c), it can be seen that the biochar particles are well dispersed in the PLA structure, while for the PLA/char 50/50 (Figure 8d), these particles are often found in clusters. The surface of the samples with biochar shows an increasing amount of plastic deformation with an increasing amount of biochar particles. The TPS image (Figure 8e) shows a smooth surface alternated with large air cavities. In the SEM image of PLA/TPS 50/50 (Figure 8f), it can be seen that the surface is more continuous without air cavities. The surface of this blend is rougher than that of pure PLA due to an increased potential for plastic deformation as compared to the pure PLA. From samples with 20 (Figure 8g) and 50 wt% (Figure 8h) of biochar, it becomes clear that also like in the PLA samples, the particles are well dispersed in the polymer structure for low concentrations of biochar, while they are more clustered at high filler loadings. The clustering of the biochar particles is in agreement with the results found from DSC and FT-IR spectroscopy.

When looking in more detail at the interfaces between the biochar particles and PLA (Figure 9a and 9b), it becomes clear that large voids are present all around the biochar particles. As more biochar particles are added, more of these voids emerge, which indicates a reduced interaction between the biochar surface and the PLA. The appearance of these voids coincides with the decreasing crystallinity of the sample, as evidenced by DSC and FT-IR results. Contrastingly, when TPS is present in the composites (Figure 9c and 9d), these voids are no longer present and are replaced by thermoplastic layers over the biochar particles, again indicating that TPS smoothens the interface between the biochar and the PLA. This observation confirms the results of both DSC and FT-IR spectroscopy, where the effects of char fillers on crystallization properties are masked in the presence of TPS.

4. Conclusions

The effect of up to 50 wt% of biochar particles in PLA/char and PLA/TPS/char samples prepared by melt compounding on the sample's composition, thermal characteristics, and crystallization behavior was investigated. It was found from TGA that biochar particles decrease the onset degradation temperature in PLA/char samples to a great extent (320 to 275 °C), while this is not the case in PLA/TPS/char samples (265 °C) due to the presence of TPS, shielding the
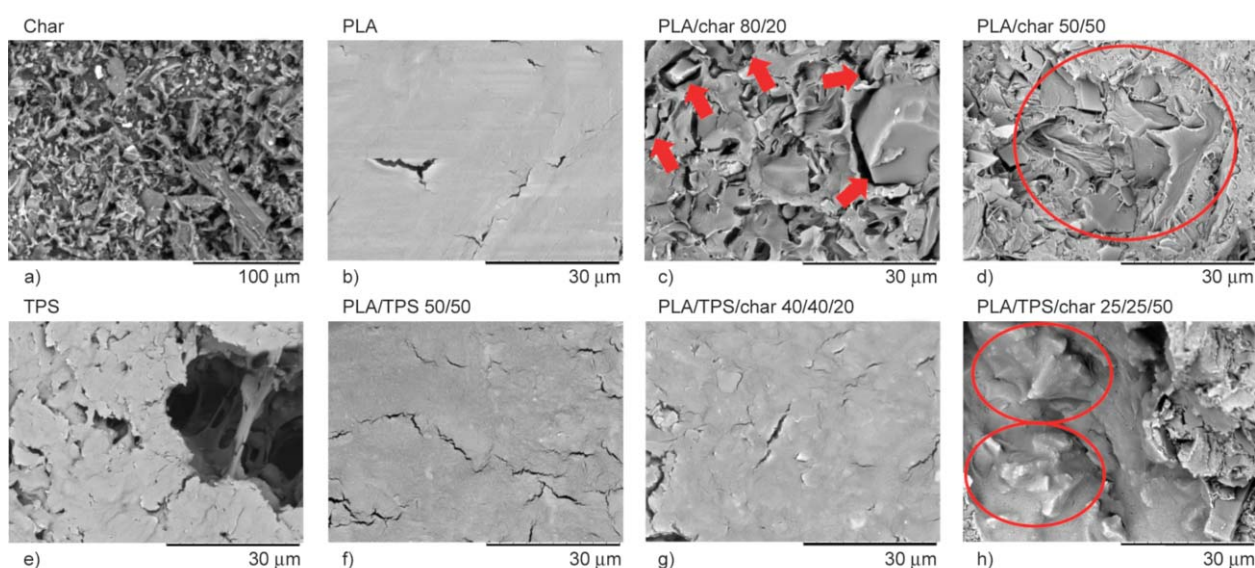
Figure 8. SEM images of char (a), PLA (b), PLA/char 80/20 (c), PLA/char 50/50 (d), TPS (e), PLA/TPS 50/50 (f), PLA/TPS/char 40/40/20 (g) and PLA/TPS/char 25/25/50 (h). Red arrows indicate biochar particles, and red circles indicate clusters of biochar particles.
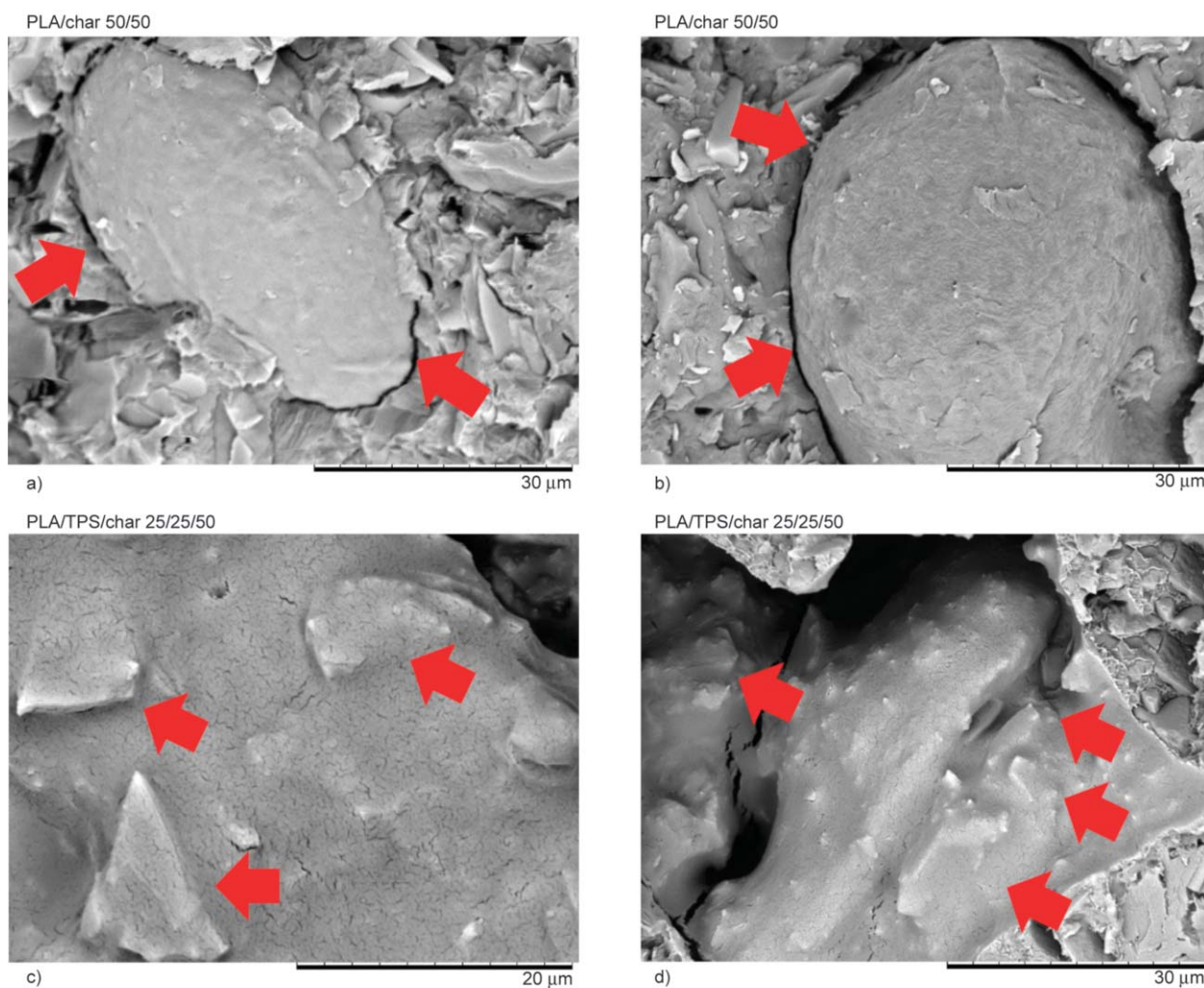
Figure 9. SEM images showing the interfaces between the char particles and polymers in PLA/char 50/50 (a and b), PLA/TPS/char 25/25/50 (c and d). Red arrows accentuate the interfaces.

effect of the biochar. From DSC, it is concluded that biochar does not influence the glass transition temperature, while TPS clearly does due to plasticization effects. Furthermore, it is found that both biochar and TPS act as a nucleation agent in crystallization. In PLA/TPS/char samples, the crystallinity remains lower than this of the PLA/char samples at low biochar concentrations (20 wt%), indicating that TPS is obstructing the nucleation effect of the char. It was found from SEM that at higher biochar concentrations (>30%), the biochar particles are more clustered, decreasing the crystallinity of the samples as found in both DSC and FTIR. From isothermal crystallization, it was found that the Avrami model fits the experimental behavior of the PLA/char samples well and that the half crystallization time keeps decreasing when more biochar particles are added to the PLA. From a comparison of the PLA/char and PLA/TPS/char samples, it can be concluded that TPS acts as an intermediator between the biochar and PLA, smoothening the interface between biochar and PLA. This result is confirmed in all TGA, DSC, FT-IR, and SEM measurements. Taking all results into account, this research gives valuable insights in the mechanistic interaction between biochar, TPS, and PLA in their respective composites and can help to further understand and optimize the release mechanisms in the future application as a slow-release fertilizer.

Acknowledgements

References

[1] Lin L., Deng C., Lin G-P., Wang Y-Z.: Super toughened and high heat-resistant poly(lactic acid) (PLA)-based blends by enhancing interfacial bonding and PLA phase crystallization. Industrial and Engineering Chemistry Research, **54**, 5643–5655 (2015).
https://doi.org/10.1021/acs.iecr.5b01177

[2] Nagarajan V., Mohanty A. K., Misra M.: Perspective on polylactic acid (PLA) based sustainable materials for durable applications: Focus on toughness and heat resistance. ACS Sustainable Chemistry and Engineering, **4**, 2899–2916 (2016).
https://doi.org/10.1021/acssuschemeng.6b00321

[3] Hashima K., Nishitsuji S., Inoue T.: Structure-properties of super-tough PLA alloy with excellent heat resistance. Polymer, **51**, 3934–3939 (2010).
https://doi.org/10.1016/j.polymer.2010.06.045

[4] Koh J. J., Zhang X., He C.: Fully biodegradable poly(lactic acid)/starch blends: A review of toughening strategies. International Journal of Biological Macromolecules, **109**, 99–113 (2018).
https://doi.org/10.1016/j.ijbiomac.2017.12.048

[5] Yuan Y., Guo M., Wang Y.: Flax fibers as reinforcement in poly(lactic acid) biodegradable composites. Communications in Computer and Information Science, **134**, 547–553 (2011).
https://doi.org/10.1007/978-3-642-18129-0_85

[6] Bax B., Müssig J.: Impact and tensile properties of PLA/cordenka and PLA/flax composites. Composites Science and Technology, **68**, 1601–1607 (2008).
https://doi.org/10.1016/j.compscitech.2008.01.004

[7] Jandas P. J., Mohanty S., Nayak S. K.: Surface treated banana fiber reinforced poly (lactic acid) nanocomposites for disposable applications. Journal of Cleaner Production, **52**, 392–401 (2013).
https://doi.org/10.1016/j.jclepro.2013.03.033

[8] Faruk O., Bledzki A. K., Fink H-P., Sain M.: Biocomposites reinforced with natural fibers: 2000–2010. Progress in Polymer Science, **37**, 1552–1596 (2012).
https://doi.org/10.1016/j.progpolymsci.2012.04.003

[9] Sánchez M. L., Patiño W., Cárdenas J.: Physical-mechanical properties of bamboo fibers-reinforced biocomposites: Influence of surface treatment of fibers. Journal of Building Engineering, **28**, 101058/1–101058/9 (2020).
https://doi.org/10.1016/j.jobe.2019.101058

[10] Siakeng R., Jawaid M., Ariffin H., Sapuan S. M.: Mechanical, dynamic, and thermomechanical properties of coir/pineapple leaf fiber reinforced polylactic acid hybrid biocomposites. Polymer Composites, **40**, 2000–2011 (2019).
https://doi.org/10.1002/pc.24978

[11] Shahzad A.: Hemp fiber and its composites – A review. Journal of Composite Materials, **46**, 973–986 (2012).
https://doi.org/10.1177/0021998311413623

[12] Battegazzore D., Noori A., Frache A.: Natural wastes as particle filler for poly(lactic acid)-based composites. Journal of Composite Materials, **53**, 783–797 (2019).
https://doi.org/10.1177/0021998318791316

[13] Dittenber D. B., GangaRao H. V. S.: Critical review of recent publications on use of natural composites in infrastructure. Composites Part A: Applied Science and Manufacturing, **43**, 1419–1429 (2012).
https://doi.org/10.1016/j.compositesa.2011.11.019

[14] Asim M., Jawaid M., Abdan K., Ishak M. R.: Effect of alkali and silane treatments on mechanical and fibre-matrix bond strength of kenaf and pineapple leaf fibres. Journal of Bionic Engineering, **13**, 426–435 (2016).
https://doi.org/10.1016/S1672-6529(16)60315-3

[15] Terpáková E., Kidalová L., Eštoková A., Čigášová J., Števulová N.: Chemical modification of hemp shives and their characterization. Procedia Engineering, **42**, 931–941 (2012).
https://doi.org/10.1016/j.proeng.2012.07.486

[16] Siakeng R., Jawaid M., Ariffin H., Sapuan S. M., Asim M., Saba N.: Natural fiber reinforced polylactic acid composites: A review. Polymer Composites, **40**, 446–463 (2019).
https://doi.org/10.1002/pc.24747

[17] Battegazzore D., Frache A., Abt T., Maspoch M. L.: Epoxy coupling agent for PLA and PHB copolymer-based cotton fabric bio-composites. Composites Part B: Engineering, **148**, 188–197 (2018).
https://doi.org/10.1016/j.compositesb.2018.04.055

[18] Li X., Shen Q., Zhang D., Mei X., Ran W., Xu Y., Yu G.: Functional groups determine biochar properties (pH and EC) as studied by two-dimensional ^{13}C NMR correlation spectroscopy. PLoS ONE, **8**, e65949/1–e65949/7 (2013).
https://doi.org/10.1371/journal.pone.0065949

[19] Batista E. M. C. C., Shultz J., Matos T. T. S., Fornari M. R., Ferreira T. M., Szpoganicz B., de Freitas R. A., Mangrich A. S.: Effect of surface and porosity of biochar on water holding capacity aiming indirectly at preservation of the amazon biome. Scientific Reports, **8**, 10677/1–10677/9 (2018).
https://doi.org/10.1038/s41598-018-28794-z

[20] Zhang Q., Zhang D., Lu W., Khan M. U., Xu H., Yi W., Lei H., Huo E., Qian M., Zhao Y., Zou R.: Production of high-density polyethylene biocomposites from rice husk biochar: Effects of varying pyrolysis temperature. Science of the Total Environment, **738**, 139910/1–139910/9 (2020).
https://doi.org/10.1016/j.scitotenv.2020.139910

[21] Poulose A. M., Elnour A. Y., Anis A., Shaikh H., Al-Zahrani S. M., George J., Al-Wabel M. I., Usman A. R., Ok Y. S., Tsang D. C. W., Sarmah A. K.: Date palm biochar-polymer composites: An investigation of electrical, mechanical, thermal and rheological characteristics. Science of the Total Environment, **619–620**, 311–318 (2018).
https://doi.org/10.1016/j.scitotenv.2017.11.076

[22] Das O., Sarmah A. K., Bhattacharyya D.: Biocomposites from waste derived biochars: Mechanical, thermal, chemical, and morphological properties. Waste Management, **49**, 560–570 (2016).
https://doi.org/10.1016/j.wasman.2015.12.007

[23] Zhang Q., Zhang D., Xu H., Lu W., Ren X., Cai H., Lei H., Huo E., Zhao Y., Qian M., Lin X., Villota E. M., Mateo W.: Biochar filled high-density polyethylene composites with excellent properties: Towards maximizing the utilization of agricultural wastes. Industrial Crops and Products, **146**, 112185/1–112185/9 (2020).
https://doi.org/10.1016/j.indcrop.2020.112185

[24] Nagarajan V., Mohanty A. K., Misra M.: Biocomposites with size-fractionated biocarbon: Influence of the microstructure on macroscopic properties. ACS Omega, **1**, 636–647 (2016).
https://doi.org/10.1021/acsomega.6b00175

[25] Nan N., DeVallance D. B., Xie X., Wang J.: The effect of bio-carbon addition on the electrical, mechanical, and thermal properties of polyvinyl alcohol/biochar composites. Journal of Composite Materials, **50**, 1161–1168 (2016).
https://doi.org/10.1177/0021998315589770

[26] Aup-Ngoen K., Noipitak M.: Effect of carbon-rich biochar on mechanical properties of PLA-biochar composites. Sustainable Chemistry and Pharmacy, **15**, 100204/1–100204/8 (2020).
https://doi.org/10.1016/j.scp.2019.100204

[27] Myllytie P., Misra M., Mohanty A. K.: Carbonized lignin as sustainable filler in biobased poly(trimethylene terephthalate) polymer for injection molding applications. ACS Sustainable Chemistry and Engineering, **4**, 102–110 (2016).
https://doi.org/10.1021/acssuschemeng.5b00796

[28] Richard S., Rajadurai J. S., Manikandan V.: Influence of particle size and particle loading on mechanical and dielectric properties of biochar particulate-reinforced polymer nanocomposites. International Journal of Polymer Analysis and Characterization, **21**, 462–477 (2016).
https://doi.org/10.1080/1023666X.2016.1168602

[29] Huber T., Misra M., Mohanty A. K.: The effect of particle size on the rheological properties of polyamide 6/biochar composites. AIP Conference Proceedings, **1664**, 150004/6–150004/10 (2015).
https://doi.org/10.1063/1.4918500

[30] Chen S., Yang M., Ba C., Yu S., Jiang Y., Zou H., Zhang Y.: Preparation and characterization of slow-release fertilizer encapsulated by biochar-based waterborne copolymers. Science of the Total Environment, **615**, 431–437 (2018).
https://doi.org/10.1016/j.scitotenv.2017.09.209

[31] González M. E., Cea M., Medina J., González A., Diez M. C., Cartes P., Monreal C., Navia R.: Evaluation of biodegradable polymers as encapsulating agents for the development of a urea controlled-release fertilizer using biochar as support material. Science of the Total Environment, **505**, 446–453 (2015).
https://doi.org/10.1016/j.scitotenv.2014.10.014

[32] Li H., Huneault M. A.: Comparison of sorbitol and glycerol as plasticizers for thermoplastic starch in TPS/PLA blends. Journal of Applied Polymer Science, **119**, 2439–2448 (2011).
https://doi.org/10.1002/app.32956

[33] Li H., Huneault M. A.: Crystallization of PLA/thermoplastic starch blends. International Polymer Processing, **23**, 412–418 (2008).
https://doi.org/10.3139/217.2185

[34] Cai J., Liu M., Wang L., Yao K., Li S., Xiong H.: Isothermal crystallization kinetics of thermoplastic starch/poly(lactic acid) composites. Carbohydrate Polymers, **86**, 941–947 (2011).
https://doi.org/10.1016/j.carbpol.2011.05.044

[35] Haeldermans T., Lataf M. A., Vanroelen G., Samyn P., Vandamme D., Cuypers A., Vanreppelen K., Schreurs S.: Numerical prediction of the mean residence time of solid materials in a pilot-scale rotary kiln. Powder Technology, **354**, 392–401 (2019).
https://doi.org/10.1016/j.powtec.2019.06.008

[36] Battegazzore D., Alongi J., Frache A.: Poly(lactic acid)-based composites containing natural fillers: Thermal, mechanical and barrier properties. Journal of Polymers and the Environment, **22**, 88–98 (2014).
https://doi.org/10.1007/s10924-013-0616-9

[37] Sawai D., Takahashi K., Imamura T., Nakamura K., Kenamoto T., Hyon S-H.: Preparation of oriented β-form poly(L-lactic acid) by solid-state extrusion. Journal of Polymer Science Part B: Polymer Physics, **40**, 95–104 (2002).
https://doi.org/10.1002/polb.10076

[38] Meaurio E., López-Rodríguez N., Sarasua J. R.: Infrared spectrum of poly(L-lactide): Application to crystallinity studies. Macromolecules, **39**, 9291–9301 (2006).
https://doi.org/10.1021/ma061890r

[39] Liu X., Wang T., Chow L. C., Yang M., Mitchell J. W.: Effects of inorganic fillers on the thermal and mechanical properties of poly(lactic acid). International Journal of Polymer Science, **2014**, 827028/1–827028/9 (2014).
https://doi.org/10.1155/2014/827028

[40] Kowalczyk M., Piorkowska E., Kulpinski P., Pracella M.: Mechanical and thermal properties of PLA composites with cellulose nanofibers and standard size fibers. Composites Part A: Applied Science and Manufacturing, **42**, 1509–1514 (2011).
https://doi.org/10.1016/j.compositesa.2011.07.003

[41] Masirek R., Kulinski Z., Chionna D., Piorkowska E., Pracella M.: Composites of poly(L-lactide) with hemp fibers: Morphology and thermal and mechanical properties. Journal of Applied Polymer Science, **105**, 255–268 (2007).
https://doi.org/10.1002/app.26090

[42] Yang Z., Peng H., Wang W.: Crystallization behavior of poly(ε-caprolactone)/layered double hydroxide nanocomposites. Journal of Applied Polymer Science, **116**, 2658–2667 (2010).
https://doi.org/10.1002/app.31787

[43] Piekarska K., Sowinski P., Piorkowska E., Haque M. M-U., Pracella M.: Structure and properties of hybrid PLA nanocomposites with inorganic nanofillers and cellulose fibers. Composites Part A: Applied Science and Manufacturing, **82**, 34–41 (2016).
https://doi.org/10.1016/j.compositesa.2015.11.019

[44] Cifuentes S. C., Frutos E., Benavente R., Lorenzo V., González-Carrasco J. L.: Assessment of mechanical behavior of PLA composites reinforced with Mg microparticles through depth-sensing indentations analysis. Journal of the Mechanical Behavior of Biomedical Materials, **65**, 781–790 (2017).
https://doi.org/10.1016/j.jmbbm.2016.09.013

[45] Ayana B., Suin S., Khatua B. B.: Highly exfoliated eco-friendly thermoplastic starch (TPS)/poly(lactic acid) (PLA)/clay nanocomposites using unmodified nanoclay. Carbohydrate Polymers, **110**, 430–439 (2014).
https://doi.org/10.1016/j.carbpol.2014.04.024

[46] Shi Q. F., Mou H. Y., Gao L., Yang J., Guo W. H.: Double-melting behavior of bamboo fiber/talc/poly (lactic acid) composites. Journal of Polymers and the Environment, **18**, 567–575 (2010).
https://doi.org/10.1007/s10924-010-0252-6

[47] Lezak E., Kulinski Z., Masirek R., Piorkowska E., Pracella M., Gadzinowska K.: Mechanical and thermal properties of green polylactide composites with natural fillers. Macromolecular Bioscience, **8**, 1190–1200 (2008).
https://doi.org/10.1002/mabi.200800040

[48] Barczewski M., Matykiewicz D., Krygier A., Andrzejewski J., Skórczewska K.: Characterization of poly(lactic acid) biocomposites filled with chestnut shell waste. Journal of Material Cycles and Waste Management, **20**, 914–924 (2018).
https://doi.org/10.1007/s10163-017-0658-5

[49] Jang W. Y., Shin B. Y., Lee T. J., Narayan R.: Thermal properties and morphology of biodegradable PLA/starch compatibilized blends. Journal of Industrial and Engineering Chemistry, **13**, 457–464 (2007).

[50] Wokadala O. C., Emmambux N. M., Ray S. S.: Inducing PLA/starch compatibility through butyl-etherification of waxy and high amylose starch. Carbohydrate Polymers, **112**, 216–224 (2014).
https://doi.org/10.1016/j.carbpol.2014.05.095

[51] Li S., Xiong Z., Fei P., Cai J., Xiong H., Tan J., Yu Y.: Parameters characterizing the kinetics of the non-isothermal crystallization of thermoplastic starch/poly (lactic acid) composites as determined by differential scanning calorimetry. Journal of Applied Polymer Science, **129**, 3566–3573 (2013).
https://doi.org/10.1002/app.38587

[52] Wang Y., He D., Wang X., Cao W., Li Q., Shen C.: Crystallization of poly(lactic acid) enhanced by phthalhydrazide as nucleating agent. Polymer Bulletin, **70**, 2911–2922 (2013).
https://doi.org/10.1007/s00289-013-0996-y

[53] Avrami M.: Kinetics of phase change. II Transformation-time relations for random distribution of nuclei. The Journal of Chemical Physics, **8**, 212–224 (1940).
https://doi.org/10.1063/1.1750631

[54] Battegazzore D., Bocchini S., Frache A.: Crystallization kinetics of poly(lactic acid)-talc composites. Express Polymer Letters, **5**, 849–858 (2011).
https://doi.org/10.3144/expresspolymlett.2011.84

[55] Lu F., Yu H., Yan C., Yao J.: Polylactic acid nanocomposite films with spherical nanocelluloses as efficient nucleation agents: Effects on crystallization, mechanical and thermal properties. RSC Advances, **6**, 46008–46018 (2016).
https://doi.org/10.1039/c6ra02768g

[56] Chen P-Y., Lian H-Y., Shih Y-F., Chen-Wei S-M., Jeng R-J.: Preparation, characterization and crystallization kinetics of kenaf fiber/multi-walled carbon nanotube/ polylactic acid (PLA) green composites. Materials Chemistry and Physics, **196**, 249–255 (2017).
https://doi.org/10.1016/j.matchemphys.2017.05.006

[57] Li S., He T., Liao X., Yang Q., Li G.: Structural changes and crystallization kinetics of polylactide under CO_2 investigated using high-pressure Fourier transform infrared spectroscopy. Polymer International, **64**, 1762–1769 (2015).
https://doi.org/10.1002/pi.4977

[58] de Araújo J. P., Silva R. C., Lima J. C. C., Agrawal P., de Mélo T. J. A.: Mechanical and thermal behavior of PLA/PEgAA blends. Macromolecular Symposia, **367**, 82–89 (2016).
https://doi.org/10.1002/masy.201500140

[59] Rocca-Smith J. R., Lagorce-Tachon A., Iaconelli C., Bellat J. P., Marcuzzo E., Sensidoni A., Piasente F., Debeaufort F., Karbowiak T.: How high pressure CO_2 impacts PLA film properties. Express Polymer Letters, **11**, 320–333 (2017).
https://doi.org/10.3144/expresspolymlett.2017.31

[60] Niazi M. B. K., Broekhuis A. A.: Surface photo-cross-linking of plasticized thermoplastic starch films. European Polymer Journal, **64**, 229–243 (2015).
https://doi.org/10.1016/j.eurpolymj.2015.01.027

[61] Pozo C., Rodríguez-Llamazares S., Bouza R., Barral L., Castaño J., Müller N., Restrepo I.: Study of the structural order of native starch granules using combined FTIR and XRD analysis. Journal of Polymer Research, **25**, 266/1–266/8 (2018).
https://doi.org/10.1007/s10965-018-1651-y

[62] Zullo R., Iannace S.: The effects of different starch sources and plasticizers on film blowing of thermoplastic starch: Correlation among process, elongational properties and macromolecular structure. Carbohydrate Polymers, **77**, 376–383 (2009).
https://doi.org/10.1016/j.carbpol.2009.01.007

[63] Mittal V., Akhtar T., Luckachan G., Matsko N.: PLA, TPS and PCL binary and ternary blends: Structural characterization and time-dependent morphological changes. Colloid and Polymer Science, **293**, 573–585 (2014).
https://doi.org/10.1007/s00396-014-3458-7

[64] Lee J. K., Lee K. H., Jin B. S.: Structure development and biodegradability of uniaxially stretched poly(L-lactide). European Polymer Journal, **37**, 907–914 (2001).
https://doi.org/10.1016/S0014-3057(00)00213-5

[65] Kizil R., Irudayaraj J., Seetharaman K.: Characterization of irradiated starches by using FT-Raman and FTIR spectroscopy. Journal of Agricultural and Food Chemistry, **50**, 3912–3918 (2002).
https://doi.org/10.1021/jf011652p

[66] Grzabka-Zasadzińska A., Klapiszewski Ł., Bula K., Jesionowski T., Borysiak S.: Supermolecular structure and nucleation ability of polylactide-based composites with silica/lignin hybrid fillers. Journal of Thermal Analysis and Calorimetry, **126**, 263–275 (2016).
https://doi.org/10.1007/s10973-016-5311-3